Acta Mech Sin (2008) 24:645–659
DOI 10.1007/s10409-008-0177-7

RESEARCH PAPER

Transient behaviors of a flame over a Tsuji burner

Young-Da Chen · Da-Da Chen · Chiun-Hsun Chen

Received: 1 August 2007 / Revised: 21 February 2008 / Accepted: 27 March 2008 / Published online: 22 July 2008

Abstract The present study investigated numerically the physical mechanisms underlying the transient behaviors of the flame over a porous cylindrical burner. The numerical results showed that a cold flow structure at a fixed inflow velocity of $U_{\text{in}} = 0.6$ m/s in a wind tunnel could be observed in two co-existing recirculation flows. Flow variations occur repeatedly until $t = 4.71$ s, and then a vortex existed steadily behind the burner and no shading occurred. The ignition of flammable mixture led to a rapid rise in gas temperature and a sudden gas expansion. When it reached the stable envelope flame condition, U_{in} is adjusted to an assigned value. Two blow-off mechanisms were identified. It was also found in the study flame shapes with buoyancy effects agreed with the ones observed experimentally by Tsai. Furthermore, the lift-off flame would appear briefly between the envelopes and wake ones, and was stabilized as a wake flame.

Keywords Tsuji burner · Lift-off flame · Recirculation flow

List of symbols

$\bar{B}$	frequency factor for gas phase reaction
C_p	average specific heat
$\bar{C}_{p\text{water}}$	specific heat of water in the water-cooling system
D	cylinder diameter
$\bar{D}$	dimensional species diffusivity
$\bar{E}$	activation energy for gas phase reaction
Le	Lewis number, $\bar{\alpha}/\bar{D}$
$\dot{m}$	mass flow rate
P	pressure
ΔP	pressure correction
Pr	Prandtl number, $\bar{\nu}/\bar{\alpha}$
$\bar{Q}$	heat of combustion per unit mass of fuel
R	radius of cylinder
T	temperature
$\bar{T}_{\text{a}}$	ambient temperature
T_{w}	non-dimensional wall temperature
T_{water}	non-dimensional water temperature in the cooling system
T^*	reference temperature
U_{in}	incoming oxidizer velocity
U	non-dimensional velocity in x-direction
V	non-dimensional velocity in y-direction
v_{w}	fuel ejection velocity through surface of cylinder
$\bar{v}_{\text{water}}$	water flow velocity in the water-cooling system
x	non-dimensional distance in x-direction
y	non-dimensional distance in y-direction
Y_{f}	mass fraction of pure methane fuel
Y_{o}	mass fraction of oxidizer
Y_{CH_4}	mass fraction of methane for methane–nitrogen and methane–air mixtures
X_{CH_4}	volume fraction of methane for methane–nitrogen and methane–air mixtures

Greek letters

α^*	thermal diffusivity at T^*
μ	dynamic viscosity
μ^*	dynamic viscosity at T^*
ν	kinematic viscosity
ρ	density

The English text was polished by Yunming Chen.

Y.-D. Chen (✉) · D.-D. Chen · C.-H. Chen
Department of Mechanical Engineering,
National Chiao Tung University, HsinChu 30056,
Taiwan, China
e-mail: chchen@mail.nctu.edu.tw

ρ^* density at T^*
$\bar{\dot{\omega}}$ reaction rate
ε_w emissivity of cylinder surface
$\bar{\sigma}$ Stefan–Boltzmann constant

Overhead

$^-$ dimensional quantities

Superscript

* reference state

Subscripts

a	ambient
f	fuel
o	oxidizer
in	inflow position
out	outflow position
n, t	normal and tangential to cylinder surface
w	surface of the porous cylinder
wall	chamber wall
water	water in the water-cooling system

1 Introduction

Many studies have extensively investigated flame behaviors over a Tsuji burner. All have emphasized the blow-off/extinction mechanisms in the forward region of a cylindrical burner. However, the corresponding flame transformation/transient behaviors have not yet been investigated. In the absence of experimental instrumentation, numerical simulation becomes a powerful tool in solving such problems.

Tsuji and Yamaoka [1–3] and Tsuji [4] conducted a series of experiments on the counterflow diffusion flame in the forward stagnation region of a porous cylinder. The corresponding extinction limits, aerodynamic effects, temperature and stable-species-concentration fields of this flame were studied in detail. They identified two flame extinction limits. The blow-off, caused by a large velocity gradient (flame stretch), occurs because of chemical limits on the combustion rate in the flame zone. However, substantial heat losses cause thermal quenching at a low fuel-ejection rate.

Tsuji and Ishizuka [5] studied a counterflow diffusion flame established in the forward stagnation region of a porous cylinder. The fuels used were methane and hydrogen, and three inert gases—nitrogen, argon and helium—were used as diluents. As the uniform oxidizer stream velocity was increased or the mixture ejection velocity was decreased, the flame approached the cylinder and was finally blown off from the forward stagnation region. As the fuel concentration in the ejected mixture or the oxygen concentration in the oxidizer stream was decreased, the flame luminosity became weaker, and finally the flame was blown off. Hasegawa et al. [6] studied numerically and experimentally the stabilization of premixed flames by a circular cylinder. They found that the volumetric expansions of premixed flames result in flashback when the flow velocity is small, and interrupt the interaction between the shear layers on both sides of the circular cylinder when the flow velocity is moderate. The existence of a liftoff flame is verified by a corresponding experimental observation [7]. The maximal liftoff height is $1.7D$ when U_{in} is 1.05 m/s, and this height is maintained up to $U_{in} = 1.09$ m/s. Then the height declines gradually as the inflow velocity increases, which is a process that can be regarded as flashback. No recirculation flow exists behind the cylindrical burner for these liftoff flames. A transition from liftoff to wake flame occurs between 1.13 and 1.15 m/s. The wake flame reappears at $U_{in} = 1.16$ m/s. Finally, the flame is extinguished completely when $U_{in} > 2.12$ m/s. The flame's lifting and dropping back is explained. Barlow et al. [8] provided a complete description of the measurements. When a laminar partially premixed methane/air flame on a Tsuji burner was used in the experiments, Raman/LIF measurements of temperature and the concentrations of the major species and NO were carried out.

The combustion model developed by Weng [9] simulated the stabilization and extinction of a flame over a porous cylindrical burner. Their model employs two-dimensional, complete Navier–Stokes momentum, energy and species equations with one-step finite-rate chemical kinetics. The adopted fuel is pure methane. He identified that the envelope, the side, and the wake flames appeared in order as the incoming flow velocity gradually increased. When the limiting value is reached, the flame is blown-off from the porous cylinder. Olson and T'ien [10] employed the global one-step chemical kinetics and adopted the simple diffusion flux expression obeying Fick's law, in which the diffusivities were the same for all species. They emphasized on the extinction limit by applying radiant heat loss to the cylinder surface, but without considering the effect of gas-phase radiation. The computed extinction boundary agrees very well with the measured extinction limits obtained by Tsuji and Yamaoka [3], except in the transition region from quenching to blowoff. However, the two aforementioned works did not compare flame structures.

This study is motivated by the study of [11], in which the envelope flame was transformed directly into a wake flame, both experimentally and numerically, when the incoming velocity gradually increased to a limiting value, in the regime of $Y_{CH_4} \leq 0.6$. However, the flame transient behaviors during flame transition were not discussed because that study adopted a steady combustion model. Therefore, the

combustion model developed by Chen et al. [11] is modified in the present study by considering the unsteady effect. The goal is to further investigate the physical mechanisms of transient flame behaviors. After the unsteady program was developed, the buoyancy effect is also taken into account to predict the flame structures accurately.

2 Mathematical model

The proposed mathematical model, from assumptions and normalization procedure to corresponding solution methodology which in itself includes a grid generation technique and algorithm, are similar to those used by Weng [9]. The major improvements are the inclusion of unsteady terms and the refinement of grid distribution. Other improvements include new boundary conditions along the wall and the buoyancy effect in the flow field. These improvements are incorporated into the corresponding simulation conditions adopted by Chen et al. [11]. Consequently, this section presents the corresponding formulae, the boundary conditions and the simulation procedure. Details of the derivation can be found in [9].

2.1 Numerical algorithm

Figure 1 shows the configuration of the flow field. The first step of the developed numerical procedure to solve the governing equations is to transform these equations to new square coordinates using a body-fitted grid generation technique, because the physical boundaries are irregular. Weng [9] detailed this procedure, which is not presented here. Throughout the computation, one of the difficulties in using the primitive variables to solve the Navier–Stokes' equations is the lack of an explicit equation for pressure. A special treatment based on the SIMPLE procedure developed by Patankar [12] is introduced to resolve the pressure gradients in the momentum equations. This work adopts a numerical procedure similar to the one used by Weng [9] with added unsteady terms. This section describes the corresponding formulae, which differs from those mentioned above. Other derivations can be found in [9].

2.2 Non-dimensional conservation equations and boundary conditions

2.2.1 Non-dimensional governing equations

Continuity equation:

$$\frac{\partial \rho}{\partial t} + \frac{\partial(\rho u)}{\partial x} + \frac{\partial(\rho v)}{\partial y} = 0. \tag{1}$$

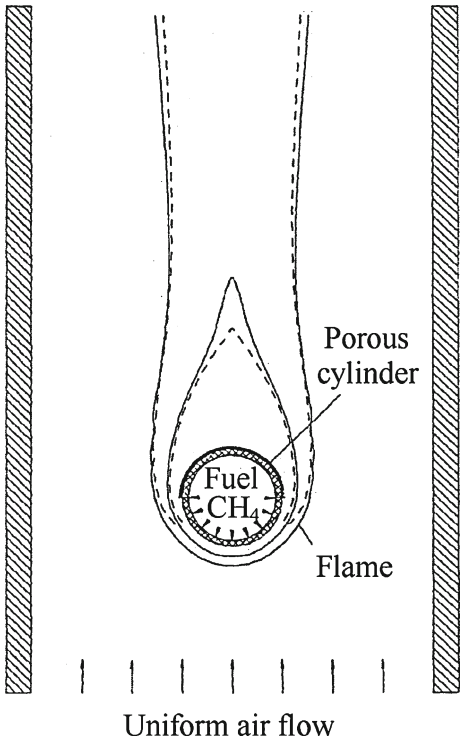

Fig. 1 Sketch of the physical problem for single burner simulation

X-momentum equation:

$$\rho\frac{\partial u}{\partial t} + \rho u\frac{\partial u}{\partial x} + \rho v\frac{\partial u}{\partial y} = -\frac{\partial p}{\partial x} + \frac{\partial}{\partial x}\left\{\frac{\mu}{Re}\left[2\frac{\partial u}{\partial x} - \frac{2}{3}\left(\frac{\partial u}{\partial x} + \frac{\partial v}{\partial y}\right)\right]\right\} + \frac{\partial}{\partial y}\left[\frac{\mu}{Re}\left(\frac{\partial u}{\partial y} + \frac{\partial v}{\partial x}\right)\right] + \frac{Gr}{Re^2}(\rho_\infty - \rho). \tag{2}$$

Y-momentum equation:

$$\rho\frac{\partial v}{\partial t} + \rho u\frac{\partial v}{\partial x} + \rho v\frac{\partial v}{\partial y} = -\frac{\partial p}{\partial y} + \frac{\partial}{\partial y}\left\{\frac{\mu}{Re}\left[2\frac{\partial v}{\partial x} - \frac{2}{3}\left(\frac{\partial u}{\partial x} + \frac{\partial v}{\partial y}\right)\right]\right\} + \frac{\partial}{\partial x}\left[\frac{\mu}{Re}\left(\frac{\partial v}{\partial x} + \frac{\partial u}{\partial y}\right)\right]. \tag{3}$$

Energy equation:

$$\rho\frac{\partial T}{\partial t} + \rho u\frac{\partial T}{\partial x} + \rho v\frac{\partial T}{\partial y} = \frac{1}{RePr}\left[\frac{\partial}{\partial x}\left(\mu\frac{\partial T}{\partial x}\right) + \frac{\partial}{\partial y}\left(\mu\frac{\partial T}{\partial y}\right)\right] - Q\dot{\omega}_f. \tag{4}$$

General species equation:

$$\rho\frac{\partial Y_i}{\partial t} + \rho u\frac{\partial Y_i}{\partial x} + \rho v\frac{\partial Y_i}{\partial y} = \frac{1}{RePrLe}\left[\frac{\partial}{\partial x}\left(\mu\frac{\partial Y_i}{\partial x}\right) + \frac{\partial}{\partial y}\left(\mu\frac{\partial Y_i}{\partial y}\right)\right] + \dot{\omega}_i, \tag{5}$$

where $\dot{\omega}_i$ represents the reaction rate of species i, which can be fuel, oxidizer, nitrogen, etc. The key reaction rate of

$$\dot{\omega}_\mathrm{f} = -Da\rho^2 Y_\mathrm{f} Y_\mathrm{o} \exp(E - E/T) \tag{6}$$

is the non-dimensional fuel reaction rate.

The equation of state is

$$\rho = 1/T \tag{7}$$

and the viscosity variation with temperature is taken as

$$\mu = T^{0.75}. \tag{8}$$

2.2.2 Non-dimensional boundary conditions

At $x = x_\mathrm{in}$:

$$u = 1, \quad v = 0, \quad T = 0.24, \quad Y_\mathrm{f} = 0, \quad Y_\mathrm{o} = 0.233. \tag{9}$$

At $x = x_\mathrm{out}$:

$$\frac{\partial u}{\partial x} = 0, \quad \frac{\partial v}{\partial x} = 0, \quad \frac{\partial T}{\partial x} = \frac{\partial Y_\mathrm{f}}{\partial x} = \frac{\partial Y_\mathrm{o}}{\partial x} = 0. \tag{10}$$

At $y = y_\mathrm{wall}$:

$$u = v = 0, \quad \frac{\partial T}{\partial y} = \frac{\partial Y_\mathrm{f}}{\partial y} = \frac{\partial Y_\mathrm{o}}{\partial y} = 0. \tag{11}$$

At $y = 0$, $x_\mathrm{in} \le x < -1$, or $1 < x \le x_\mathrm{out}$

$$\frac{\partial u}{\partial y} = 0, \quad v = 0, \quad \frac{\partial T}{\partial y} = \frac{\partial Y_\mathrm{f}}{\partial y} = \frac{\partial Y_\mathrm{o}}{\partial y} = 0. \tag{12}$$

At $-1 < x \le 0$ and $\sqrt{x^2 + y^2} = 1$

$$\begin{aligned} &v_\mathrm{t} = 0, \quad v_\mathrm{n} = \text{assigned value}, \ \dot{m}_\mathrm{w} = v_\mathrm{n}\rho_\mathrm{w} \\ &\dot{m}_\mathrm{w}(T_\mathrm{w} - T_\mathrm{a}) = \frac{1}{RePr}\mu\frac{\partial T}{\partial n}\bigg|_\mathrm{w} - F_0\varepsilon_\mathrm{w}(T_\mathrm{w}^4 - T_\mathrm{a}^4), \\ &\quad -\rho_\mathrm{water} C_{p_\mathrm{water}} V_\mathrm{water}(T_\mathrm{w} - T_\mathrm{water}), \\ &\dot{m}_\mathrm{w}(Y_{\mathrm{CH_4 w}} - 1) = \frac{1}{RePrLe}\mu\frac{\partial Y_{\mathrm{CH_4}}}{\partial n}\bigg|_\mathrm{w}, \\ &\dot{m}_\mathrm{w} Y_\mathrm{ow} = \frac{1}{RePrLe}\mu\frac{\partial Y_\mathrm{o}}{\partial n}\bigg|_\mathrm{w}. \end{aligned} \tag{13}$$

At $0 < x \le 1$ and $\sqrt{x^2 + y^2} = 1$

$$\begin{aligned} &v_\mathrm{t} = 0, \quad v_\mathrm{n} = 0, \\ &\frac{1}{RePr}\mu\frac{\partial T}{\partial n}\bigg|_\mathrm{w} = F_0\varepsilon_\mathrm{w}(T_\mathrm{w}^4 - T_\mathrm{a}^4) \\ &\quad +\rho_\mathrm{water} C_{p_\mathrm{water}} V_\mathrm{water}(T_\mathrm{w} - T_\mathrm{water}), \\ &\frac{\partial Y_\mathrm{f}}{\partial n}\bigg|_\mathrm{w} = 0, \quad \frac{\partial Y_\mathrm{o}}{\partial n}\bigg|_\mathrm{w} = 0. \end{aligned} \tag{14}$$

2.3 Simulation procedure

The simulation procedure follows Tsai's experiment [13], which is an extension of the experiment carried out by Chen et al. [11]. Accordingly, the whole combustion process is divided into four steps. The first step is to generate a steady flowfield at a low inlet velocity, $U_\mathrm{in} = 0.6$ m/s. For the initial conditions, the velocity and pressure are assumed to be zero and the temperature is assumed to be 300 K. After 10 s, the fuel and methane begin to be ejected into the incoming air flow from the forward half of a Tsuji burner with

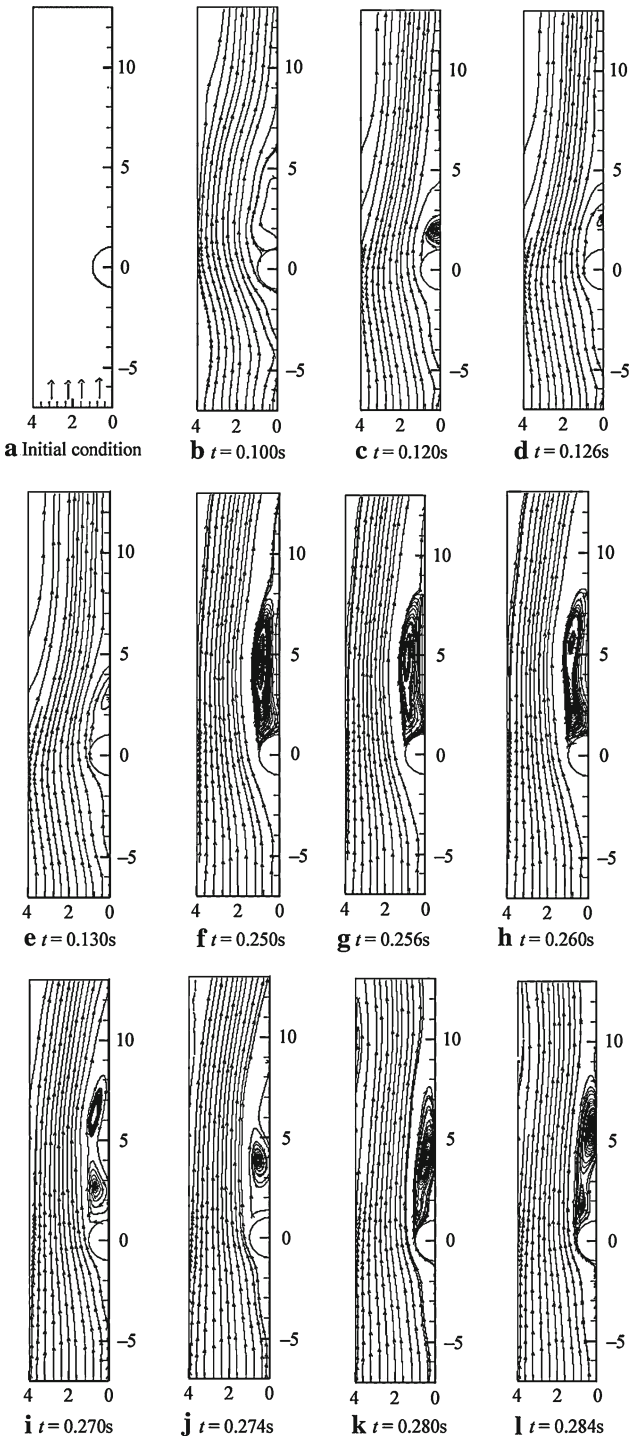

Fig. 2 Series of streamline contour distributions when the inflow velocity $U_\mathrm{in} = 0.6$ m/s ($Re = 572.52$)

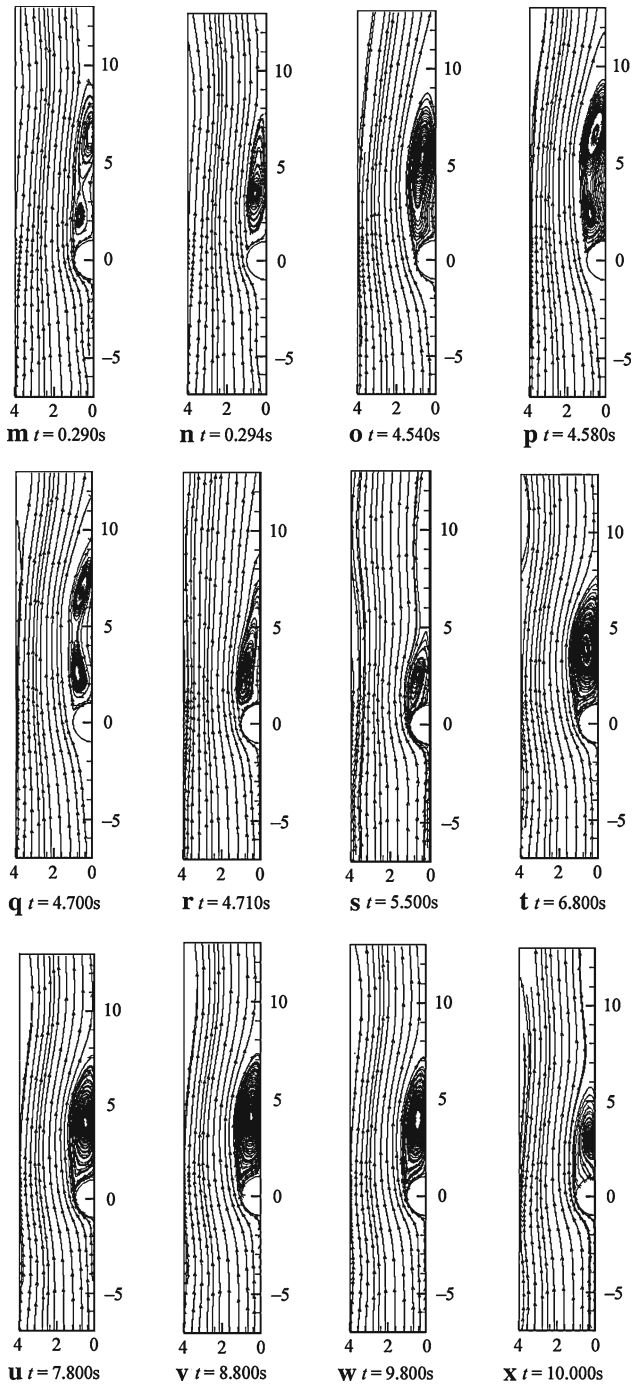

Fig. 2 continued

$V_w = 0.05$ m/s. In the second step, the initial distributions of velocity and pressure are given as those simulated values at 10 s from the beginning, and the temperature is still assumed to be 300 K. The boundary conditions for the velocities, fuel and oxidizer are those given in Sect. 2.2.2. A heat source is imposed to generate an ignition and subsequently the flame. The initial conditions of velocity, pressure and species in the third step, ignition, follow the corresponding distributions obtained 0.05 s after the second step. As the flame becomes a stable envelope flame, the inflow velocity is gradually adjusted to a desired value, according to the formula, $U_{in} = 0.6 + kt$. The rate of variation, k, is determined by the increased value in velocity of the blower, which accelerates the flow velocity from 0.6 to 1.16 m/s in 4.7 s of Tsai's experiment [13]. The initial conditions in the fourth step are set as the computed values at 2.8 s after ignition because the flame and flow structures, including flame shape, the thickness and the recirculation flow are almost invariant with time. The governing equations used in the third and fourth steps are exactly the same as the ones described in Sect. 2.2.1. The boundary conditions are exactly the same as those described in Sect. 2.2.2.

3 Results and discussion

As mentioned above, the combustion model is modified and different from that of [11] by adding unsteady terms. The purpose is to investigate the physical mechanisms underlying the transient behaviors of the flame. After accomplishing the development of unsteady program, the buoyancy effect is also taken into account to predict the flame structures more accurately, and respective simulation results are discussed below.

3.1 Case without buoyancy effect

In the steps for generating a cold premixed flow, the reference values adopted were those of ambient atmosphere. In the other steps, the thermodynamics, transport, and chemical kinetic data were nearly identical to those used by Weng [9].

3.1.1 Flow structure in the cold flow

Figure 2 shows the history of a series of streamline contours at an inflow velocity of $U_{in} = 0.6$ m/s. The time step used for this computation is 0.002 s. Just after the start-up of the inflow, shown in Fig. 2a, the streamlines behind the Tsuji burner are deflected toward the centerline as shown in Fig. 2b, since a reverse pressure gradient is generated by the air flow passing over the cylindrical burner, and no recirculation flow occurs at that moment. As time proceeds, the flow can no longer follow the sharp turning at the rear edge of the cylindrical burner; accordingly, a recirculation flow forms at $t = 0.12$ s as shown in Fig 2c. Then, the recirculation flow is gradually brought toward the downstream of the wind tunnel and disappears, as shown in Fig. 2d and e. At $t = 0.25$ s, the recirculation flow reappears behind the burner. Then, it is also brought toward the downstream region and disappears. However, another recirculation flow is forming behind the burner as the former recirculation flow has not completely died out yet. Figure 2 f–j show this process. It can be observed that two recirculation flows co-exist in the wind tunnel, as

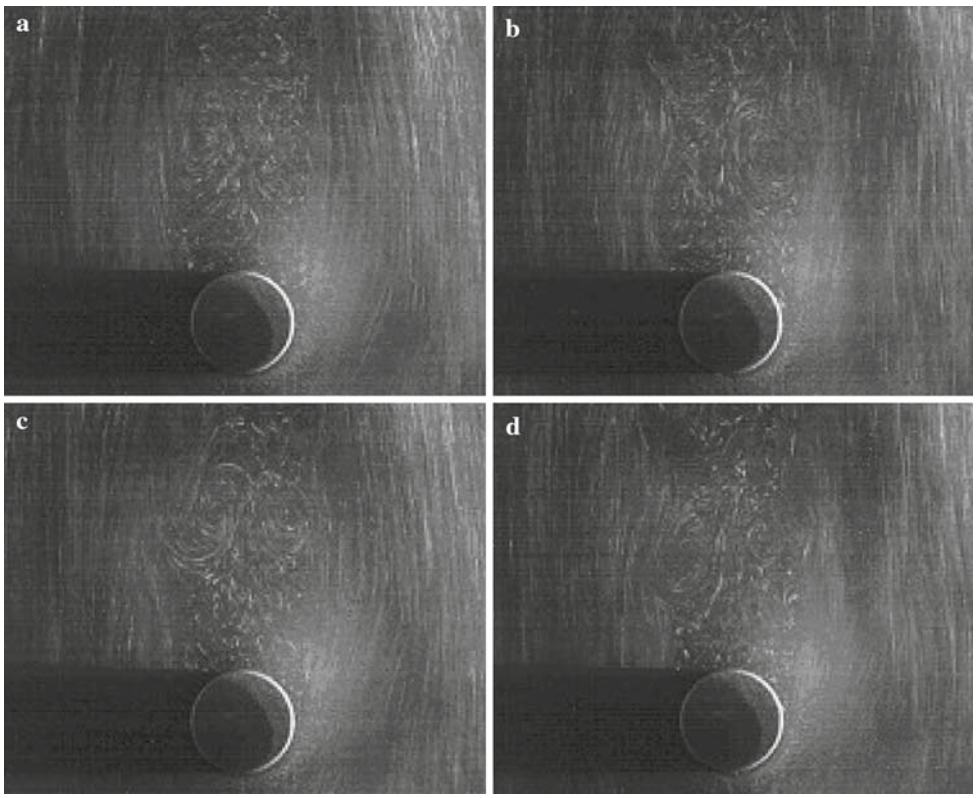

Fig. 3 Series of experimental photographs of streamline contour distributions when the inflow velocity $U_{in} = 0.6$ m/s ($Re = 572.52$). **a** $t = 0.233$ s; **b** $t = 0.267$ s; **c** $t = 0.300$ s; **d** $t = 0.333$ s

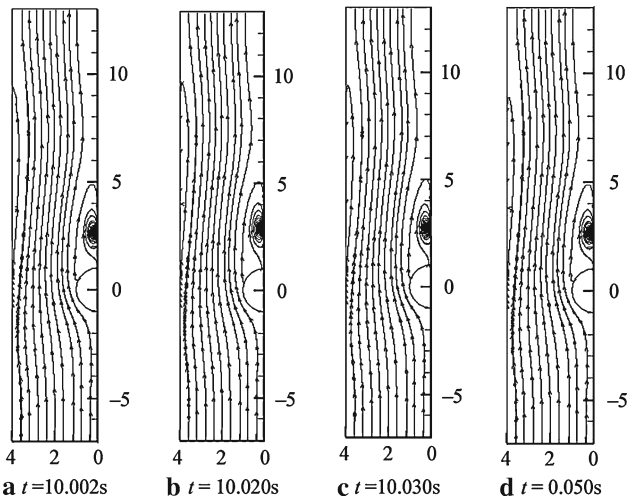

Fig. 4 Series of streamline contour distributions in the case of fuel ejection with an inflow velocity $U_{in} = 0.6$ m/s ($Re = 572.52$)

shown in Fig. 2 h and i. The flow variations, shown in Fig. 2 g–j, occurs repeatedly until $t = 4.71$ s. After that, the vortex exists steadily behind the burner and no shading occurs. The computation is carried out until $t = 10$ s.

Figure 3 shows photographs of the cold flow taken in the experiment under the same conditions as used in the numerical simulation. They are obtained using a PIV (particle image video) system with an exposure time of 1/30 s. More detailed results will be published in the future. The flow variations shown in Fig. 3 a–d are quite similar to those predicted results shown in Fig. 2 g–j, and the trend will always repeat. However, the flow variations on the left side and the right side in the photographs taken during the experiment are not symmetric, whereas the simulation assumes symmetry about the centerline. However, the perturbation caused by the seeding of small scattering particles would influence the uniformity of the inlet flow and lead to unsymmetry. It should be noted that photographs cannot be taken before 0.3 s because the particles have not yet reached the desired position. Furthermore, the photographic process can last 5 s only, because the supply of seeding particles is limited.

When the fuel and methane, is ejected into the incoming air flow at $t = 10$ s from the forward half of a Tsuji burner with $V_w = 0.05$ m/s, the resultant flows are almost invariant with time, as shown in Fig. 4, and thus a stable flowfield can be considered to exist. However, if the interval between the fuel ejection and ignition is too long, the flame at ignition is certainly unstable and more time is needed to form a stable envelope flame.

3.1.2 Transient behavior from ignition to formation of stable envelope flame

Figure 5 displays combinations of isotherms and streamlines; the lines on the left side represent isotherms and the lines on the right side represent streamlines. Figure 6 displays

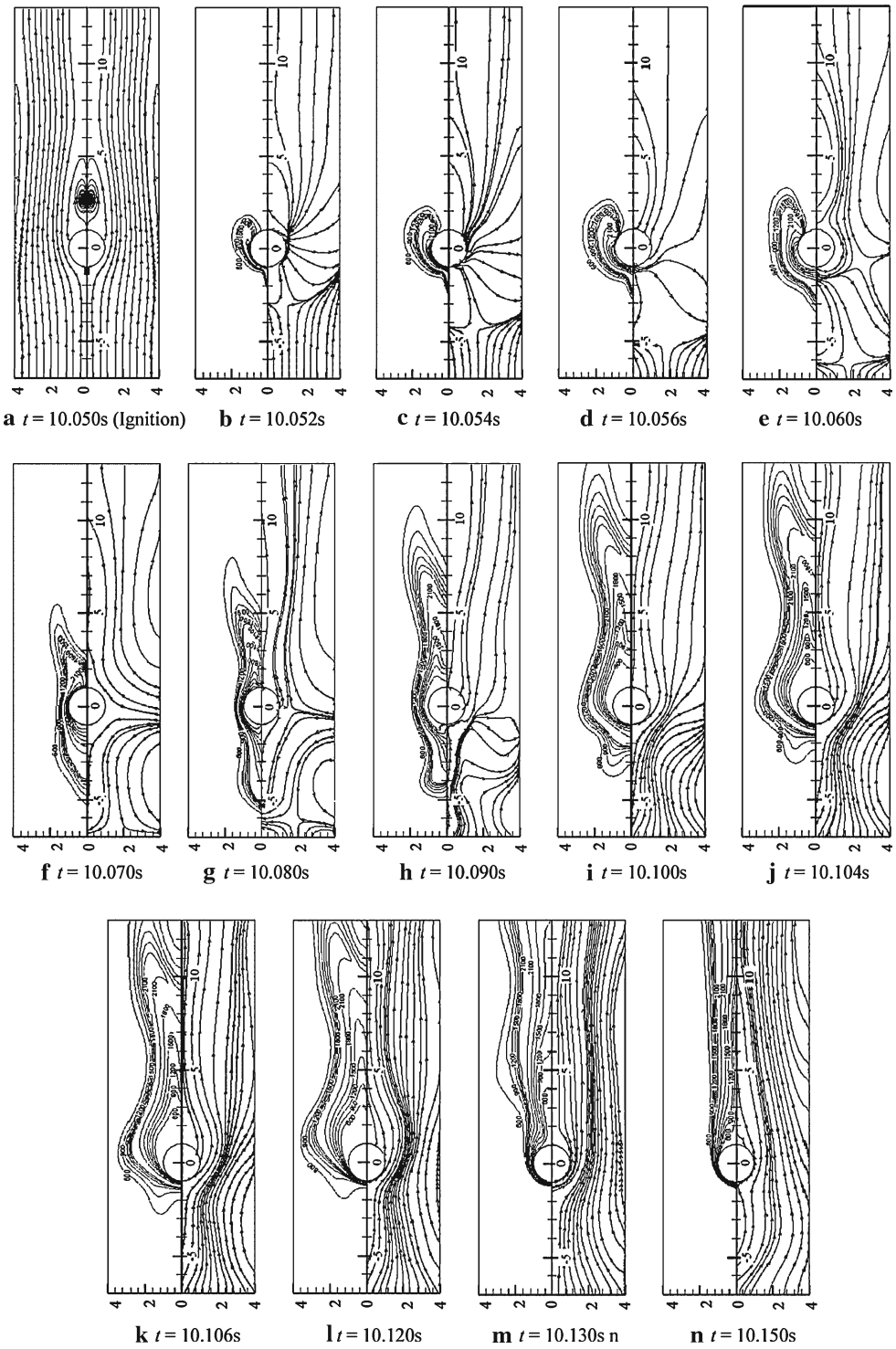

Fig. 5 Series of temperature and streamline contour distributions at the instant of ignition with an inflow velocity $U_{\text{in}} = 0.6$ m/s ($Re = 53.25$)

corresponding combinations of fuel and oxidizer mass fractions as well as reaction rate distributions. The black lines in the left-hand picture of Fig. 6 represent flame boundaries. The gray lines on the left-hand side of the right-hand picture represent methane mass fraction distributions. The silver gray lines on the right-hand side of the right-hand picture represent oxidizer mass fraction distributions. They are used to describe the transient behaviors at the instant of ignition when the inflow velocity, U_{in}, is 0.6 m/s.

At the beginning, $t = 10.05$ s, a heat source is imposed on the steady flow field to trig the ignition. The area of the imposed heat source is represented by the black region in front of the cylindrical burner, as shown in Fig. 5a, with a height of $0.06R$ and a length of $0.55R$. The temperature of

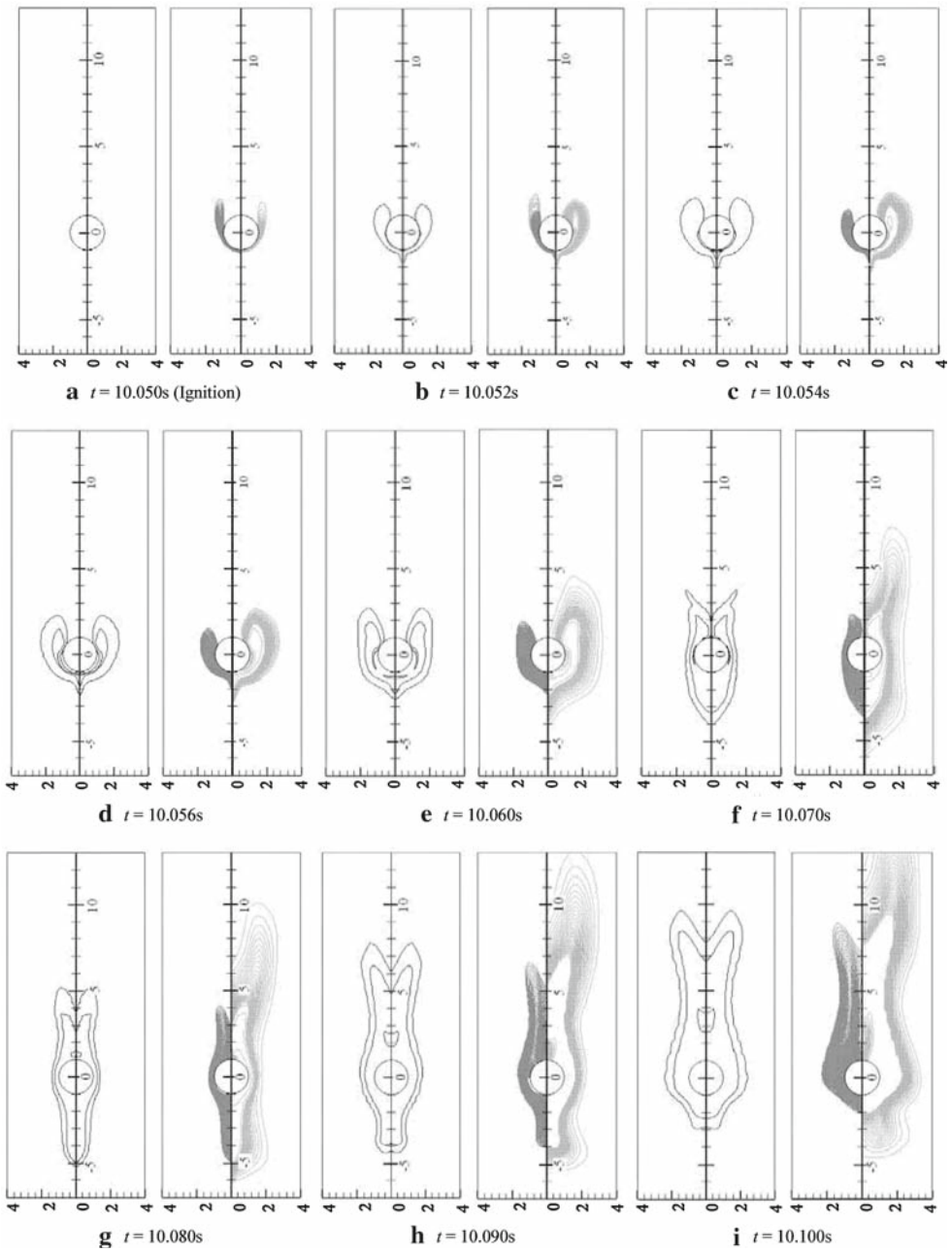

Fig. 6 Series of fuel and oxidizer mass fraction and reaction rate distributions at the instant of ignition with an inflow velocity $U_{\text{in}} = 0.6$ m/s ($Re = 53.25$)

the heat source is set as 1,000 K, and the ignition duration is one time step, which is 0.002 s. Figure 6a, which combines fuel and oxidizer distributions at $t = 10.05$ s, reveals that the fuel and oxidizer have been fully premixed around the burner before ignition.

The air–fuel mixture reacts to produce a flame when the heat source is imposed. After the instant of ignition, an active chemical reaction occurs along the cylindrical burner, releasing a large amount of heat, rapidly increasing the gas phase temperature, causing a sudden gas expansion. The reacting region enlarges rapidly, as shown in Fig. 6b ($t = 10.052$ s)–e ($t = 10.06$ s). The temperature contours vary similarly, as shown in Fig. 5b–e. Meanwhile, the incoming flow ahead of the flame front is retarded by the adverse pressure gradient generated by the gas thermal expansion. The thermal expansion also contributes to the outward deflection of the incoming flow, as shown in Fig. 5b–g (10.08 s). Additionally, the rapid rise in the gas phase temperature creates a strong induced flow concurrent with the forced flow moving toward the downstream of the wind tunnel. Some of the ejected fuel

Fig. 6 continued

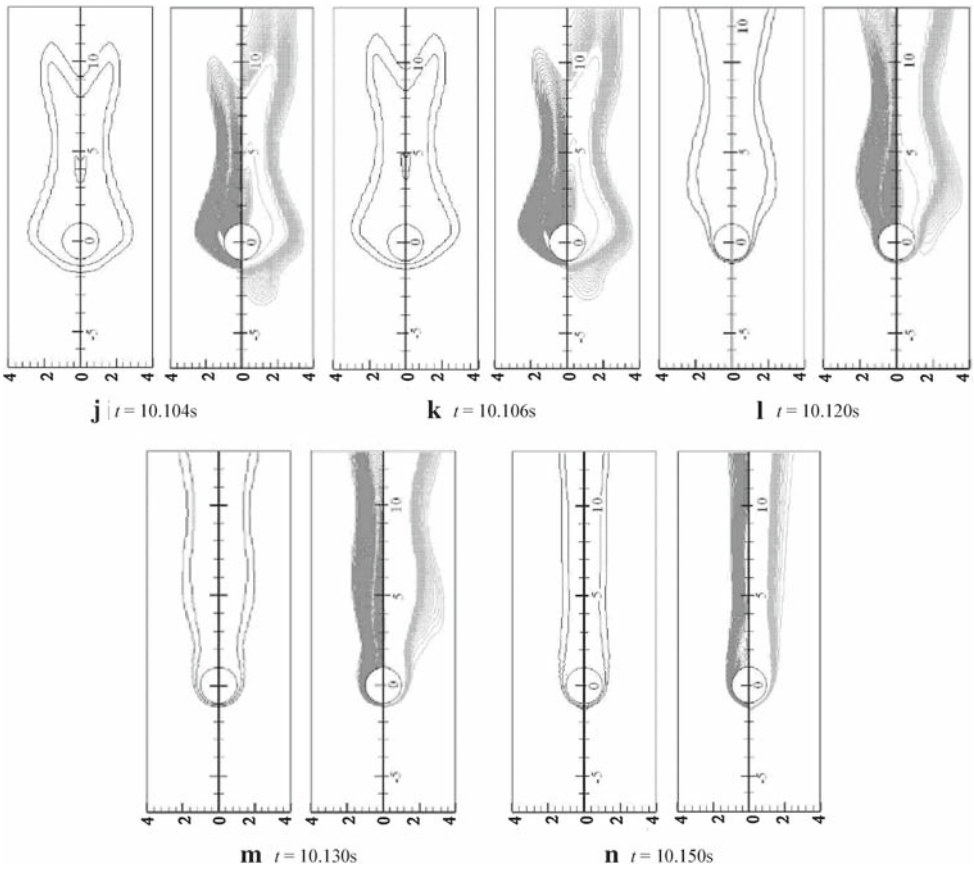

moves upstream due to the convection of ejected fuel; the rest of the fuel flows downstream along with the main stream. Then, the fuel is continuously mixed with air and the ignition is kept on because the temperature in the reaction zone is high, and the flame spreads upstream and downstream accordingly along the burner, as shown in Figs. 5f (10.07 s)–h (10.09 s) and 6f–h.

Figure 6b and f reveal the fact that the premixed gas mixture is gradually consumed. In other words, the flame is transformed from a premixed flame to a diffusion flame. At $t = 10.08$ s, the premixed gas mixture in the flame front is almost completely burned out, as shown in Fig. 6g. As the time proceeds, the effect of gas thermal expansion is gradually reduced. Hence, the fuel originally accumulated ahead of the burner and ejected from the forward half of the cylindrical burner will be brought downstream of the wind tunnel by the convective effect of the incoming flow.

Figure 7 shows the corresponding experimental photographs taken during the ignition process, as mentioned above. They are obtained using a high-speed camera. Figure 7 also shows that the flame initially moves upstream, and then retreats and develops into an envelope flame. However, the flame variations on the left and right of the experimental photographs are not symmetric because the ignition point in the experiment is at the right-hand side of the burner and not at the center, whereas the simulation assumes symmetry about the centerline.

3.1.3 Inflow effect

In this step, the initial conditions are set as the stable envelope flame conditions, which are the simulation results at 2.8 s after ignition at a fixed $U_{\text{in}} = 0.6$ m/s. Now, the inflow velocity, U_{in}, will be adjusted to an assigned value. The inflow velocity varies according to the formula $U_{\text{in}} = 0.6 + kt$. In that formula, k is determined according to the rate of increase of the velocity of the blower, which increased approximately 0.56 m/s in 4.7 s in the experiment of [13].

Figure 8 displays combinations of isotherms and streamlines; the lines on the left side represent isotherms and the lines on the right side represent streamlines. Figure 9 displays a series of 10^{-4} g/(cm^3 s) fuel reaction rate contours represented by the black lines at various inflow velocities. Figures 8a–c and 9a–c show that as inflow velocity gradually increases, the flame is pushed closer to the burner surface and the flame zone becomes thinner, because an increase in incoming airflow velocity intensifies the convection and stretch effects that push the flame toward the burner surface and make the flame thinner.

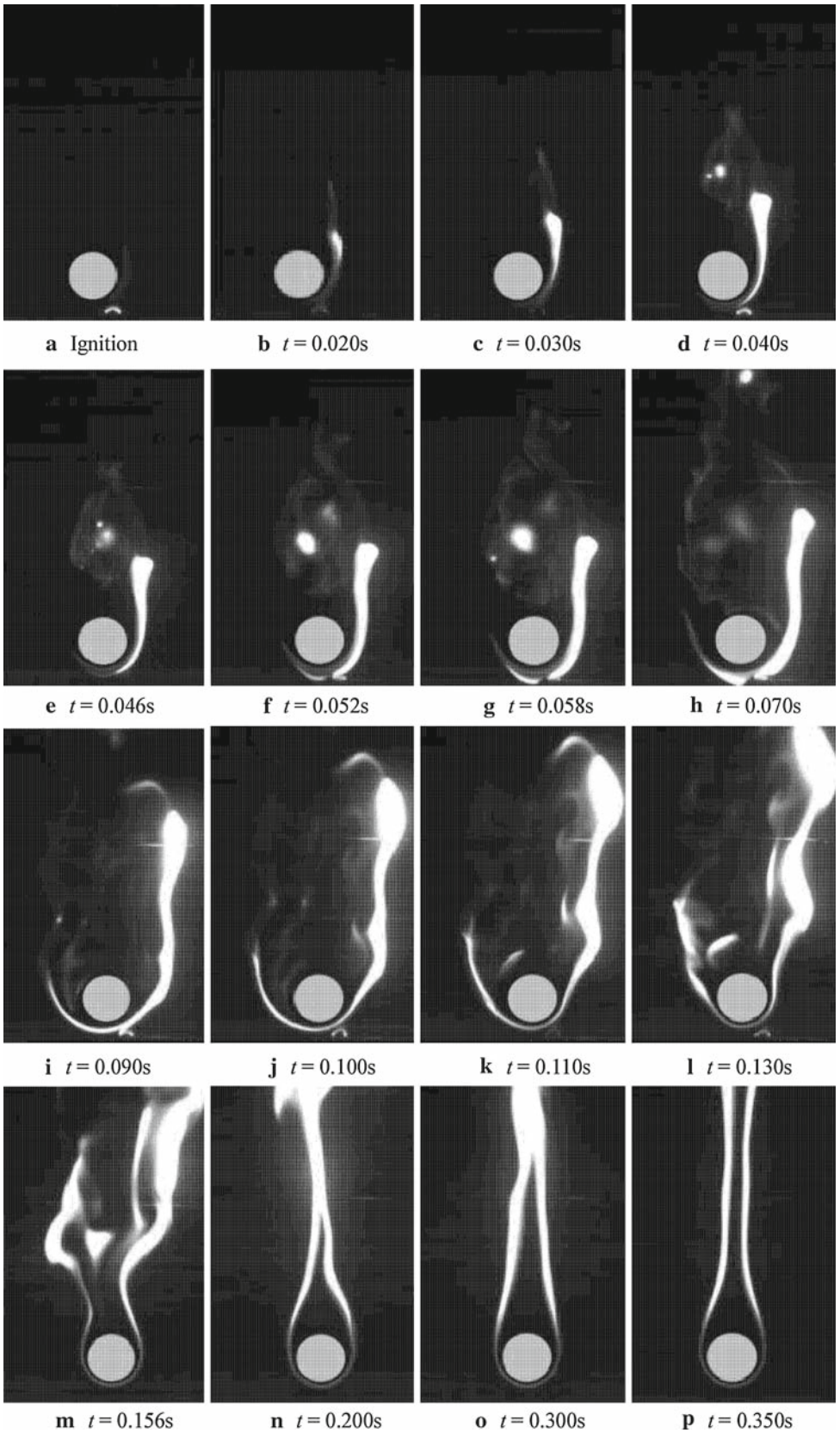

Fig. 7 Series of experimental photographs of flame shapes at the instant of ignition with an inflow velocity $U_{\text{in}} = 0.6$ m/s ($Re = 53.25$)

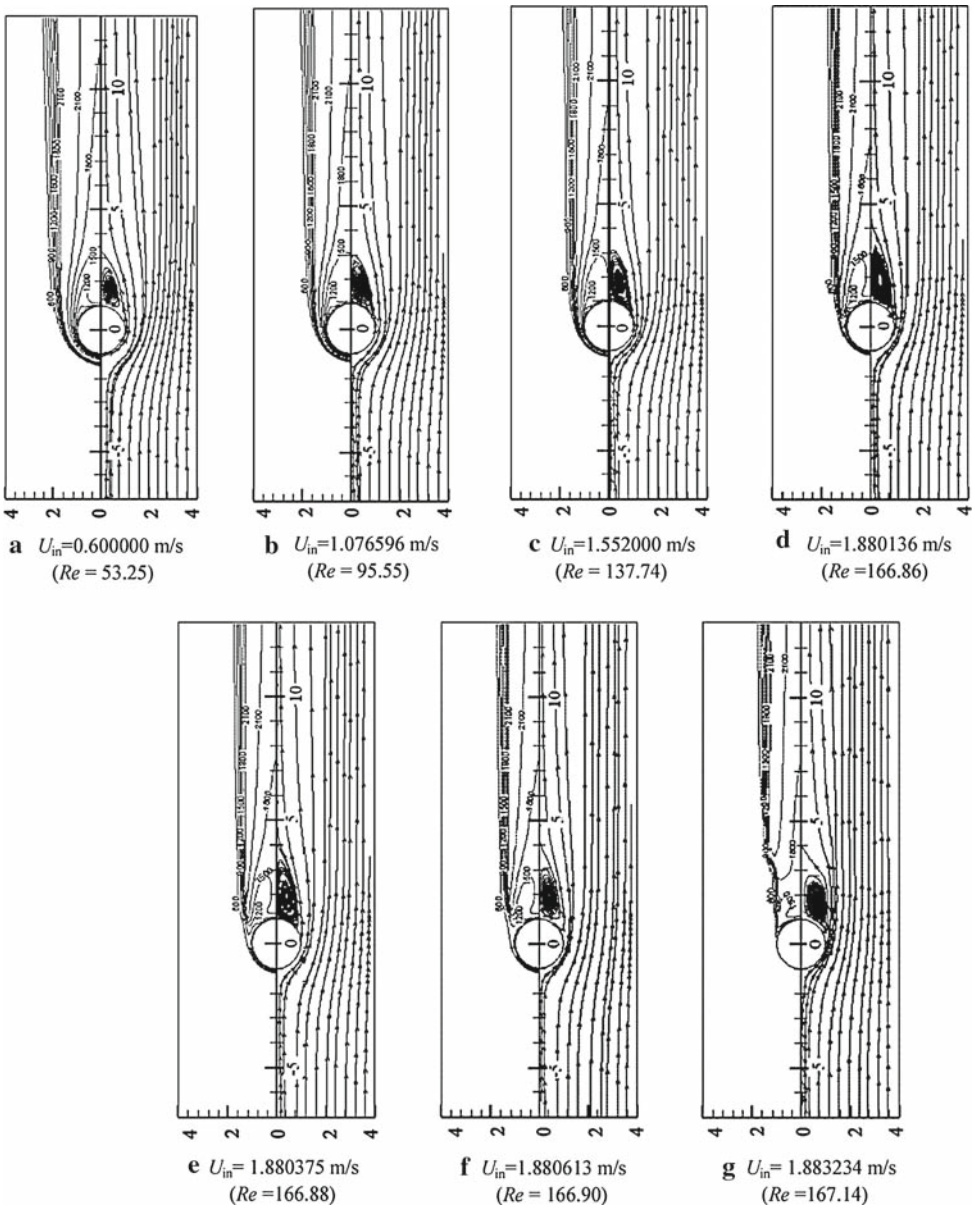

Fig. 8 Temperature and streamline contour distributions at various inflow velocities

Figures 8d–f and 9d–f show that as the inflow velocity increases to a limit, $U_{in} = 1.880136$ m/s to 1.880375 m/s, the flame zone can no longer withstand the strong flame stretch, hence, the reaction zone will be cut off. The reaction zone does not connect to the rear surface of the burner and the flame front disappears gradually. Additionally, the recirculation flow is also separated from the burner as the reaction zone is pulled to separate from the burner, because the temperature in that region falls, leading to a smaller volumetric expansion. Figure 10 shows the photographs of flame transient behaviors at the instant of the breakage of the envelope flame front in Tsai's experiments [13]. Figure 10 reveals the fact that the flame is cut off, and then the flame front disappears gradually.

Figures 8f and g and 9f and g show that the flame gradually approaches the rear surface of burner. As the inflow velocity, U_{in}, increases above 1.883234 m/s, the reaction zone is connected to the rear surface of burner, because as the inflow velocity increases gradually, more air is brought from upstream, and thus the flame is reinforced.

3.1.4 Comparisons with Chen et al. [11]

In [11], the predicted blow-off limit is a little lower than that observed experimentally. However, the predicted blow-off limit should be larger because the one-step overall chemical kinetics combustion model is adopted. The major reason for this discrepancy is believed to be the preheating effect

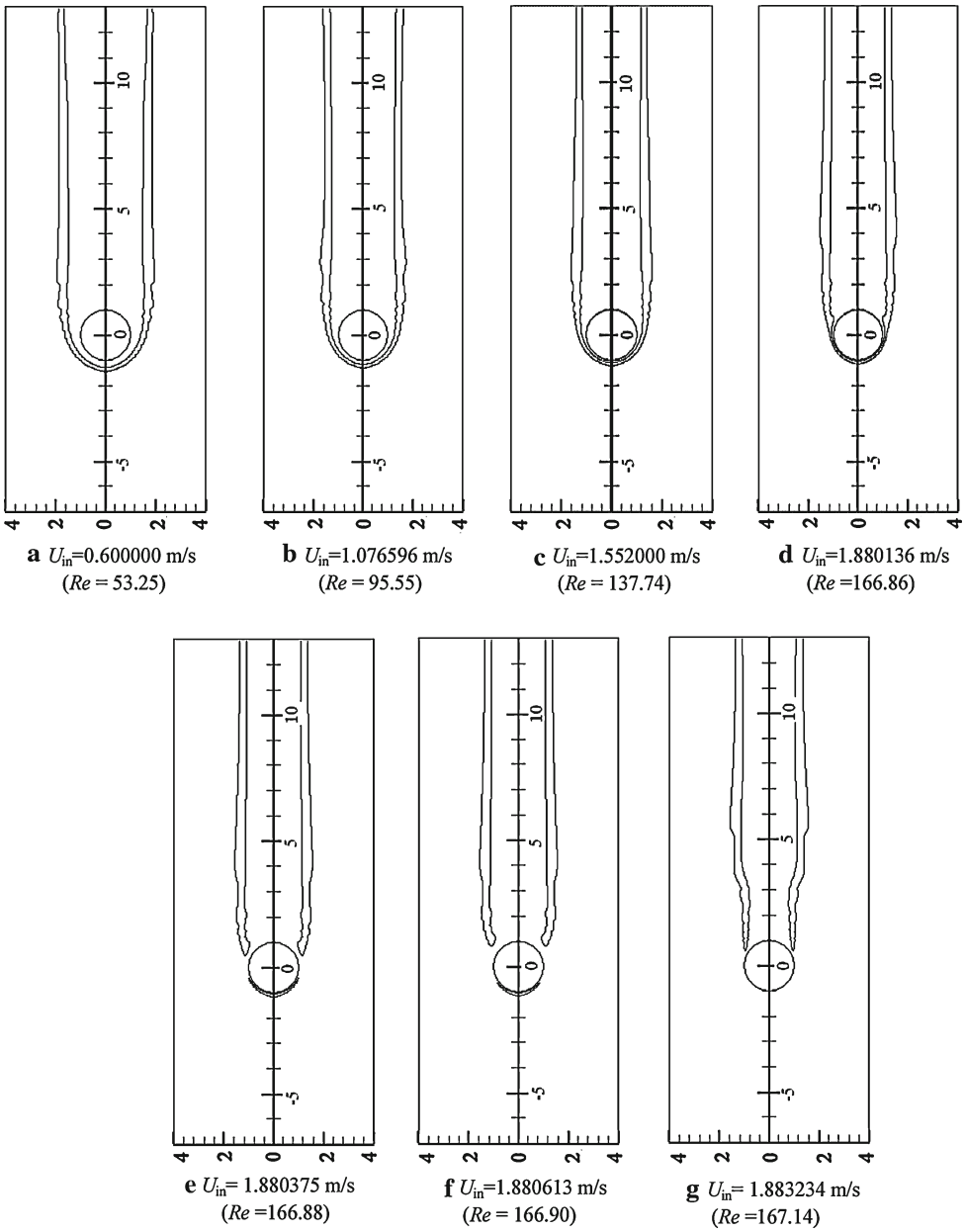

Fig. 9 Flame boundaries, 10^{-4} g/(cm^3 s) methane reaction rate contours at various inflow velocities

of incoming flow, which is not considered in the combustion model. In this study, the unsteady model considers the preheating effect of incoming flow. The predicted velocity is U_{in} = 1.880375 m/s, which exceeds the value obtained experimentally by Chen et al. [11]. Additionally, the predicted results in [11] can only depict an elementary flame structure and phenomenon analyses, but cannot describe the flame transient behaviors. In this study, the flame transient behaviors can be described because of the adoption of an unsteady model. Although the unsteady simulation finds only that the reaction zone is interrupted and separated from the rear surface of the burner, no lift-off flame is identified as the incoming velocity increases to a limiting value. The separation distance between the reaction zone and the rear surface of the burner is smaller than that obtained numerically and experimentally by Tsai [13]. As stated above, the main reason is the preheating effect of the incoming flow, which is considered in the present model and expected to strengthen the flame and highlight the effect of the assumption of overall one-step chemical kinetics.

3.2 Buoyancy effect

In this case, the buoyancy term is incorporated into the unsteady combustion model. This effect is elucidated by comparisons between the results predicted with and without buoyancy. The parametric studies are based on variations of inflow velocity. The flame shape and flame transition velocity

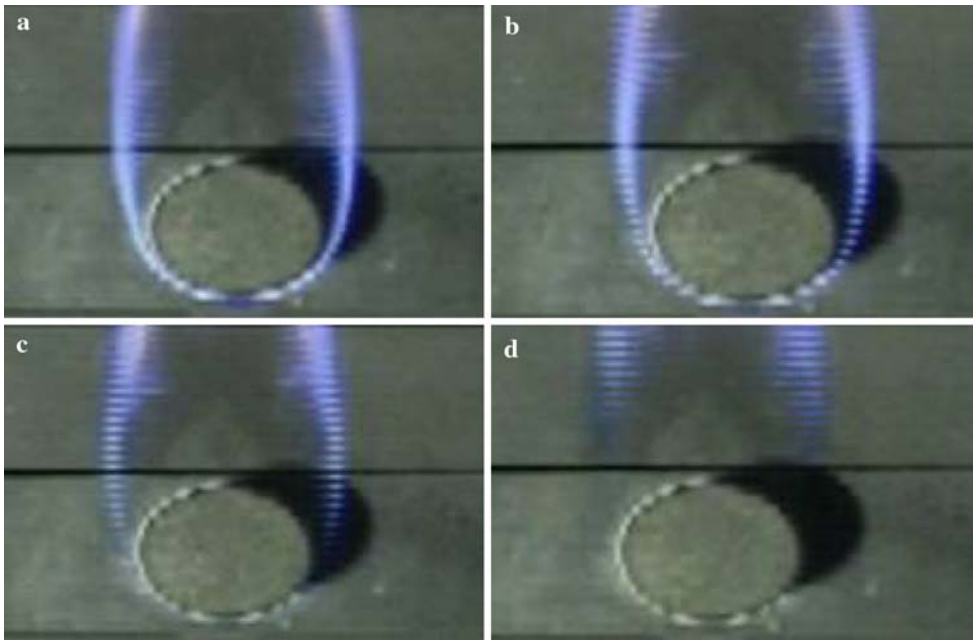

Fig. 10 Series of Tsai's experimental photographs showing flame transient behavior. Where $t = 0$ represents the time when the envelope flame structure starts to convert. **a** $t = -0.333$ s; **b** $t = 0.000$ s; **c** $t = 0.333$ s; **d** $t = 0.666$ s

are compared. The corresponding results and discussion are as follows.

Figure 11 shows a series of predicted flame shapes at various inflow velocities. In every case, the left part is the predicted flame shape with buoyancy and the right one is the prediction without buoyancy. This figure shows that when buoyancy is not considered, the wake of the predicted flame extends upright, whereas when buoyancy is considered, the wake of the predicted flame shrinks toward the centerline. As the inflow velocity increases, the discrepancy decreases. A comparison with the results observed by Tsai [13], as shown in Fig. 12, indicates that the flame shape predicted with buoyancy seems to be in closer agreement with the experimental value of [13] than that without, as expected. As the inflow velocity increases, the ratio of natural convection to forced convection becomes smaller, and the discrepancy becomes smaller accordingly. However, the predicted degree of contraction of the flame wake is smaller than that observed by Tsai [13]. This discrepancy may be attributed to the assumption of overall one-step chemical kinetics in the numerical combustion model, which would strengthen the combustion. Therefore, the natural convection due to thermal buoyancy influences the wake of the flame less. The resultant blow-off limit, $U_{\text{in}} = 1.858928$ m/s, obtained by considering the buoyancy effect is lower than that obtained without considering the buoyancy effect.

Figure 13 shows a series of combinations of flame structures and 10^{-4} g/(cm^3 s) fuel reaction rate contours obtained by considering the buoyancy effect when the envelope flame is transformed into the wake flame, where the left part represents the flame structure and the right one represents the 10^{-4} g/(cm^3 s) fuel reaction rate contours. Figure 13c and e show that the predicted separation distance from the burner to the top of the reaction zone when buoyancy is considered, exceeds the prediction when the buoyancy effect is not considered. The lift-off flame appears briefly between the envelope and the wake flame. This is because the induced flow is generated by thermal buoyancy. However, a comparison with the experimental observations of [13] reveals that the predicted separation distance is smaller than the experimental observation. This discrepancy may be attributed to the overall one-step chemical kinetics assumption adopted in the numerical combustion model. Of course, the neglected three-dimensional effect may also contribute to the discrepancy.

4 Conclusions

This study indicated that the flow structure in cold flow has co-existing recirculation flows in the wind tunnel at an inflow velocity of $U_{\text{in}} = 0.6$ m/s. Just after the start-up of the inflow, the streamlines behind the Tsuji burner are deflected toward the centerline, because of the reverse pressure gradient generated by the air flow passing over the cylindrical burner, and the fact that no recirculation flow occurred at that moment. As time proceeds, the flow can no longer follow the sharp turning at the rear edge of the cylindrical burner, and thus the formed recirculation flow is gradually brought toward the downstream of the wind tunnel and disappears, and then the recirculation flow reappears behind the burner. It can be observed that two recirculation flows co-exist in the wind tunnel. The flow variation repeatedly occurs until $t = 4.71$ s. After that, a vortex exists steadily behind the burner and no shading occurs. When the fuel, methane, is ejected into the

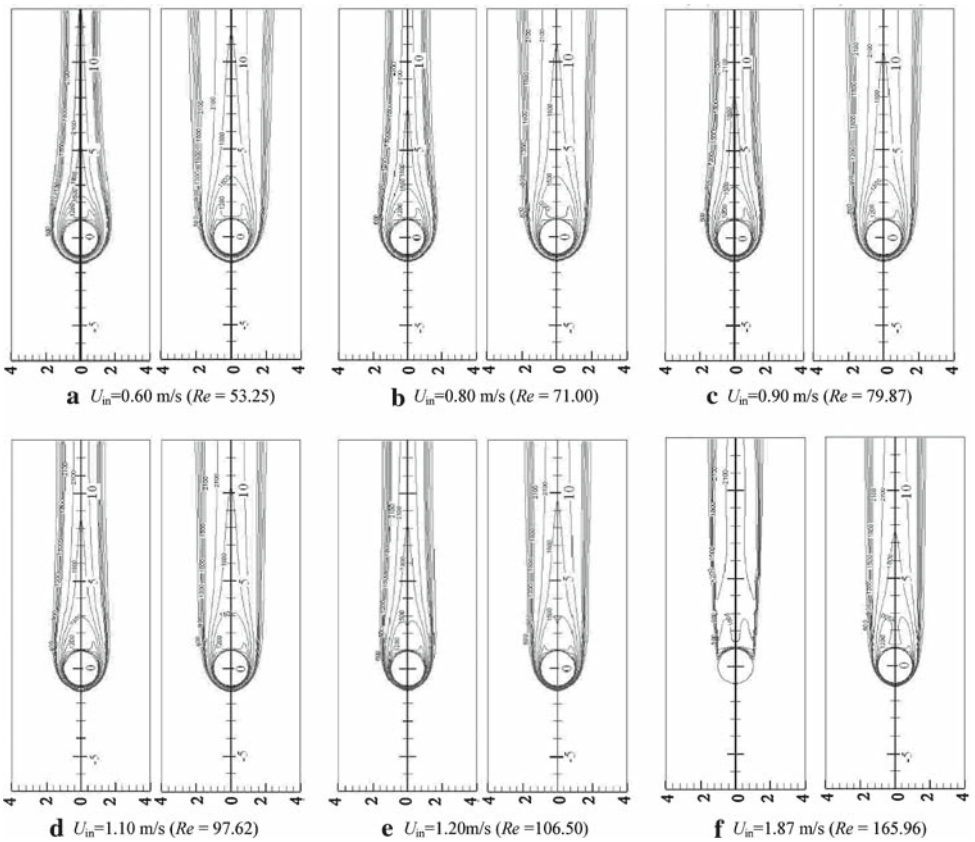

Fig. 11 Flame shapes at various inflow velocities, where the *left* part is the flame shape considering buoyancy effect and the *right* is the flame shape without the buoyancy effect

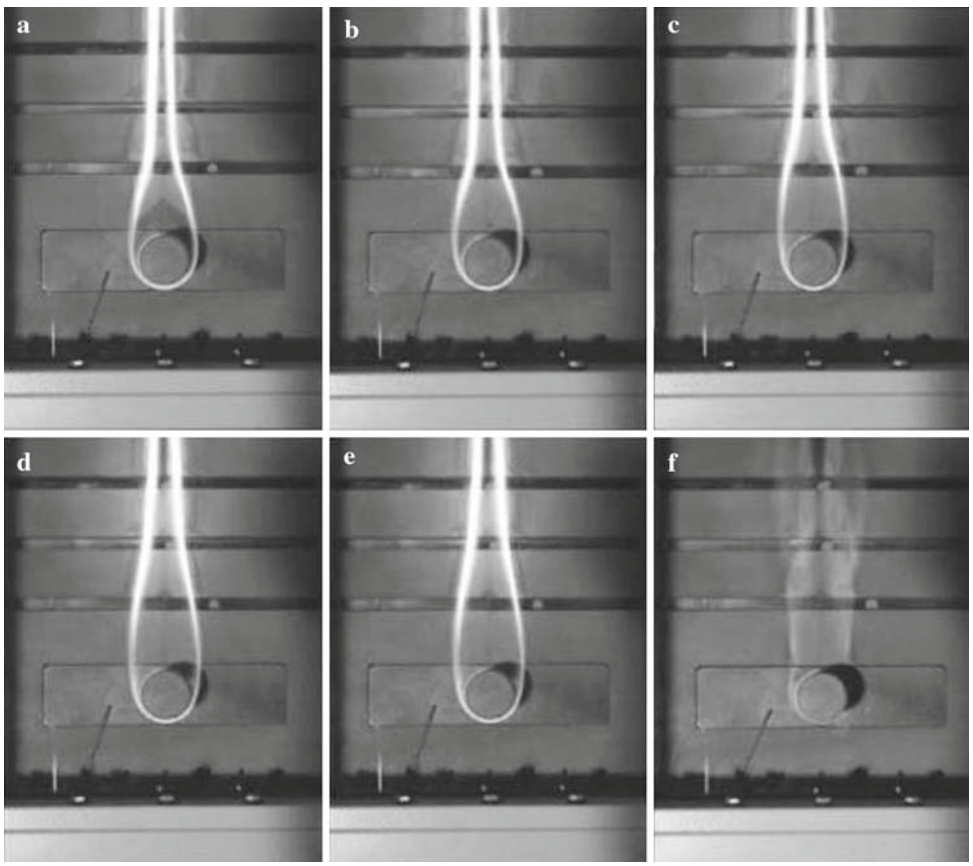

Fig. 12 Flame shapes observed by Tsai [13] at various inflow velocities. **a** $U_{in} = 0.60$ m/s ($Re = 53.25$); **b** $U_{in} = 0.80$ m/s ($Re = 71.00$); **c** $U_{in} = 0.90$ m/s ($Re = 79.87$); **d** $U_{in} = 1.10$ m/s ($Re = 97.62$); **e** $U_{in} = 1.20$ m/s ($Re = 106.50$); **f** $U_{in} = 1.87$ m/s ($Re = 165.96$)

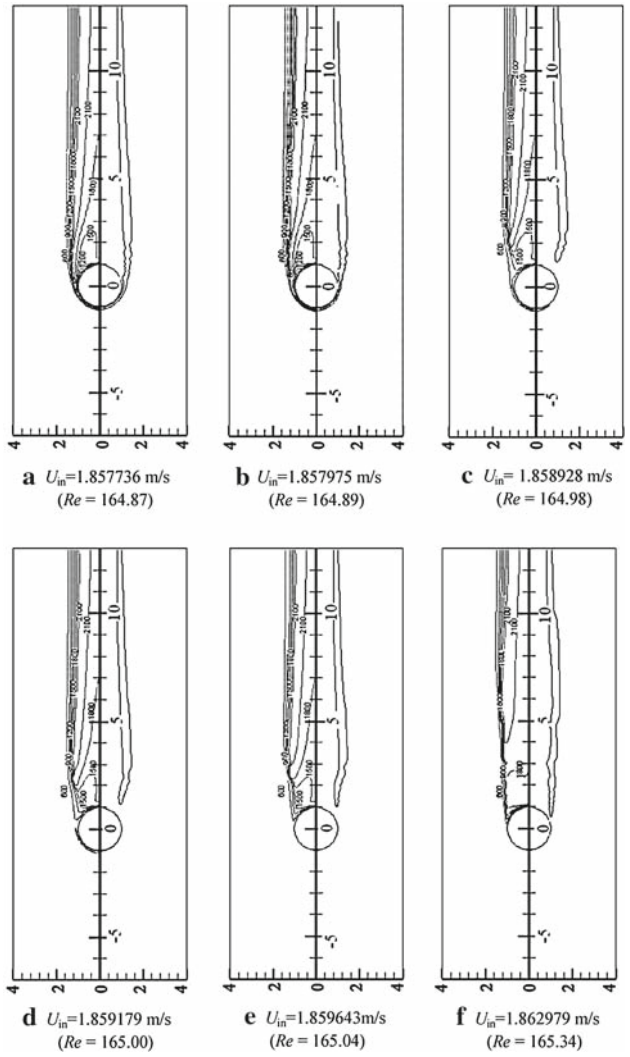

Fig. 13 Flame shapes at various inflow velocities when the flame transits

incoming air flow from the forward half of a Tsuji burner with $V_w = 0.05$ m/s, the resultant flows are almost invariant with time.

As the flammable mixture is ignited, a large amount of heat is release, leading to a rapid rise in gas phase temperature and a sudden gas expansion. Then, the incoming flow ahead of the flame front is retarded due to the adverse pressure gradient generated by the gas thermal expansion. The rapid rise in the gas phase temperature creates a strong flow concurrent with the forced flow moving downstream of the wind tunnel. The flame spreads upstream and downstream along the burner. As time passes, the effect of gas thermal expansion falls gradually. The flame retreats gradually and develops into an envelope diffusion flame. When a stable enveloped flame is present, the inflow velocity , U_{in}, is adjusted to an assigned value. The two extinction mechanisms, quenching and flame stretch, are identified. As inflow velocity increases to a limit, the reaction zone is cut off and the flame front disappears gradually.

Comparisons between the predicted results with buoyancy and those without buoyancy indicates that the former are in closer agreement with the flame shapes observed experimentally by Tsai [13]. Additionally, the lift-off flame occurs briefly between the envelope and the wake flames, and then the wake flame becomes stabilized. So far, the model emphasizes only the aeordynamic effect on flame extinction for a given one-step chemical kinetics. The consideration of multistep chemical reactions are believed to be very important and necessary for cases near the extinction limits, although its inclusion in the model would cause a lot of complexities, such as the use of multicomponent diffusion fluxes and diffusion fluxes and the interchange of mass and molar fractions, etc.

References

1. Tsuji, H., Yamaoka, I.: The counterflow diffusion flame in the forward stagnation region of a porous cylinder. In: Eleventh Symposium (International) on Combustion, The Combustion Institute, Pittsburgh (1967)
2. Tsuji, H., Yamaoka, I.: The structure of counterflow diffusion flame in the stagnation region of a porous cylinder. In: Twelfth Symposium (International) on Combustion, The Combustion Institute, Pittsburgh (1969)
3. Tsuji, H., Yamaoka, I.: Structure analysis of counterflow diffusion flames in the forward stagnation region of a porous cylinder. In: Thirteenth Symposium (International) on Combustion (1971)
4. Tsuji, H.: Counterflow diffusion flame. Prog. Energy Combust. Sci. **8**(2), 93–119 (1982)
5. Tsuji, H., Ishizuka, S.: An experimental study of effect of inert gas on extinction of lamina diffusion flames. In: Eighteenth Symposium (International) on Combustion, pp. 695–703 (1981)
6. Hasegawa, T. et al.: The discrete vortex simulation premixed flame by a circular cylinder. Trans. Jpn. Soc. Mech. Eng. **57**, 533 (1986)
7. Tsa, S.S., Chang, C.C., Chen, C.H.: Experimental visualizations of counterflow diffusion flame over a porous cylindrical burner. Accepted for publication in J. Chin. Soc. Mech. Eng. (2003)
8. Barlow, R.S., Karpetis, A.N., Frank, J.H., Chen, J.Y.: Scalar profiles and no formation in laminar opposed-flow partially-premixed methane/air flames. Combust. Flame **127**, 2102–2118 (2001)
9. Weng, F.B.: Diffusion flame stabilization and blowoff over a porous cylinder. M.S. thesis, National Chiao Tung University, Taiwan, China (1989)
10. Olson, S.L., T'ien, J.S.: A theoretical analysis of the extinction limits of a methane-air opposed-jet diffusion flame. Combust. Flame **70**, 161–170 (1987)
11. Chen, D.D., Chen, C.H.: The flame transition analyses for methane-nitrogen fuels over a Tsuji burner. In: Proceedings of the 5th Asai-Pacific Conference on Combustion, pp. 313–316 (2005)
12. Patankar, S.V.: Numerical Heat Transfer and Fluid Flow. Mcgraw-Hill, New York (1980)
13. Tsai, Y.C.: The experimental analyses of counter-flow diffusion flame over tsuji burner—the effects of methane diluted with nitrogen. M.S. thesis, National Chiao Tung University, Taiwan, China (2005)